A Coupled Cluster Approach to Computationally Design an Acid Catalyst for Viable Release of H_2 from BN Nanotubes

Lisa Roy[1]

Correspondence to: l.roy@iocb.ictmumbai.edu.in

[1]*Institute of Chemical Technology Mumbai, IOC Odisha Campus Bhubaneswar, IIT Kharagpur Extension Centre, Bhubaneswar, India, 751013*

ABSTRACT

Catalytic removal of H_2 from boron-nitride (BN) based nanomaterials at ambient conditions is of paramount importance in order to develop light-weight hydrogen storage media. Herein, the DLPNO-CCSD(T) technique is used for calculating accurate relative energies and activation barriers of Brønsted acid-initiated removal of H_2 from hydrogenated BN nanotubes (HBNNTs) with several *in silico* designed catalysts. Three crucial steps are identified in the mechanism: 1st H_2 release, catalyst regeneration via proton transfer and 2nd H_2 release to ensure feasibility of the dehydrogenation proposal. Our computational studies reveal that sulfonic acids with appropriate electron withdrawing substituents can facilitate dehydrogenation of HBNNT at a low free energetic cost ($\Delta G^{\ddagger}$ = 17 kcal mol^{-1}). Importantly, these findings illustrate reversibility of hydrogen stored in BN nanomaterials at room conditions and raises hope for a sustainable chemical hydrogen storage strategy.

Introduction

Identification of a safe and efficient hydrogen storage method is an impediment in the development of a hydrogen-based renewable energy technology.[1] Recent years have witnessed a fervent search towards the design and development of appropriate on-board hydrogen storage systems with high gravimetric (5.5 wt% H_2) and volumetric capacity (4.0 vol% H_2) of H_2 which operates in the temperature range of - 40 to + 60 °C.[2-5] Promising storage technologies include physisorption over extended network families like metal organic frameworks (MOFs) [6] and chemisorption over functionalized and nanostructured graphene sheets.[7] However, the adsorption enthalpy of H_2 on pore surfaces of MOFs are rather low (-5 to -12 kJ mol^{-1}), under optimum temperature pressure conditions, which preclude MOF based hydrogen repositories.[8] Furthermore, multi-layered graphene sheets with controlled interfacial spacing are considered as practical solutions for hydrogen storage but are challenging to prepare compared to the epitaxial sheets studied by most research groups.[9] Alternatively, chemical hydrogen storage in compounds primarily composed of light elements like boron and nitrogen are also attractive because they exhibit appreciable hydrogen content at ambient temperatures.[10] Among them, ammonia borane (AB) has been touted as a chemical hydrogen storage system due to its high gravimetric content of hydrogen (19.6 wt% H_2) and low molecular weight (30.7 g/mol).[11] Naturally, this also elicits curiosity in the reactivity of this fascinating molecule and on its related polymeric materials.[12-17] While the ease of hydrogen release from AB either thermally or with various catalysts is advantageous,[13,18] its practical application is limited by the unsolved problem of regeneration from the spent fuel.[19] Notably, boron and nitrogen containing light-weight allied materials like boron nitride nanotubes (BNNTs), nanocages and fullerenes are also investigated as promising hydrogen storage media owing to their large

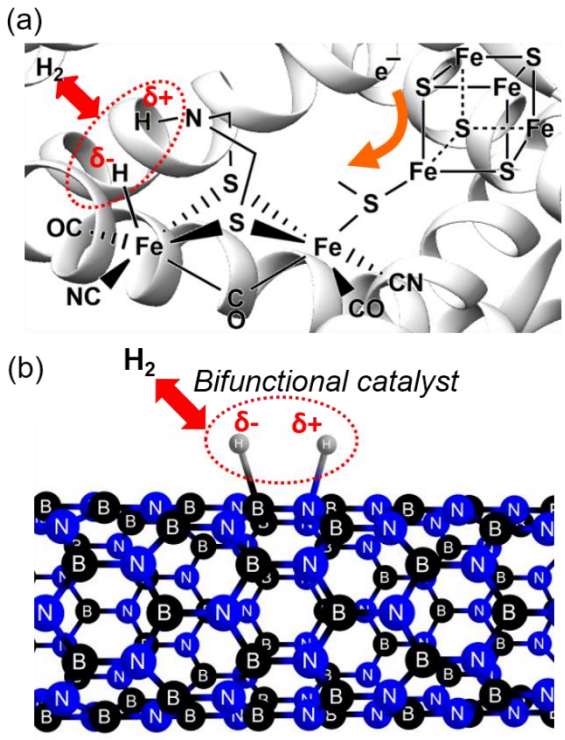

Figure 1. Reversible H_2 release (a) in the active site of the [FeFe] hydrogenase and (b) from HBNNT aided by a bifunctional catalyst

surface area for greater chemisorption.[20-26] Mutated structures, for e.g. bamboo-like (2.6 wt% H_2)[20] and collapsed (4.2 wt% H_2)[21] BNNTs can store hydrogen gas at room temperature and maximum allowed pressure of 10 MPa. Furthermore, recent works also demonstrate excellent adsorption of H_2 up to 5.6 wt% on boron nitride whiskers at room temperature and reduced pressure of 3 MPa.[26] This has renewed interest in BN based novel materials for hydrogen storage.[27] However, realization of a hydrogen economy out of these BN nanomaterials (> 350 °C), or graphene and hydrogenated carbon nanotubes (500 °C) is curtailed by the high thermal desorption temperature.[20,21] Notably, practical storage media should comply with the reversible mechanism of hydrogenation and dehydrogenation to ensure sustainability of the hydrogen delivery cycle. Albeit, development of catalytic approaches for H_2 release from hydrogenated BNNTs (HBNNTs) with fast kinetics under ambient conditions would surely be an advancement towards a sustainable chemical hydrogen storage strategy. Although the literature is rife with theoretical studies on hydrogenation of BNNTs, BN fullerenes and other relevant BN nano-structures, identification of low-barrier channels to release dihydrogen molecules with application of appropriate reagents or catalysts is a rather challenging task.[27] Indeed, release of H_2 at room temperature from these storage materials would be an appreciable feat.

Bi-functional activation of H_2 are profound in biological domains like in the active site structure of hydrogenase and cytochrome c oxidase enzymes which selectively and reversibly furnish H_2 (Figure 1a).[28] Similarly, in a recent communication, we proposed that bi-functional reagents with optimum proton and hydride acceptors can ensue dehydrogenation from HBNNTs because of the unique disposition of both protic (δ+) and hydridic (δ-) hydrogen atoms attached to N and B centers, respectively (Figure 1b).[29] Thus, we found that hydrogenated BN nanotubes and fullerenes chemically behave in a similar fashion as ammonia borane or in general as amine boranes.[29] This spurred up the possibility of dehydrocoupling of chemisorbed hydrogens on HBNNTs at activation energies surmountable at room temperatures. Embarking on this knowledge, in a preceding report we proposed that trifluoro methanesulphonic acid, popularly known as triflic acid, could be employed to catalytically release H_2 from HBNNTs.[30,31] However, our previous theoretical study indicated that regeneration of this organic acid and further removal of H_2 from the nanotube surface is a rather difficult process, occurring at predicted barriers of 22 - 24 kcal/mol which suggest that consequential desorption of H_2 would take place with a modest inflation in temperature (~ 40 – 50 °C).[30] Inspired by the several reports on transition metal based

catalytic systems for dehydrogenation of amine boranes,[12,13,18,32-33] we explored the possibility of removal of H_2 from HBNNT with some of the premier organometallic catalysts.[34] However, we realized that other than bis-phosphinite di-hydride Ir complex [(POCOP)Ir(H)$_2$],[18] where POCOP = [η^3-1,3-(OP^{t}Bu$_2$)$_2$C$_6$H$_3$], most of the catalysts like the Fe pincer complex designed by Guan *et. al.*,[32] Ruthenium catalyst designed by Williams and group,[33] Baker's Ni(NHC)$_2$ systems[12] were ineffective to initiate H_2 release from the surface of HBNNT due to significant steric encumbrance between the bulky phenyl substituents on the catalysts and the curved nanotube surface. Here we would like to note that all of these catalysts had favorable interaction with the protons and hydrides of ammonia borane. Although, the computationally identified iridium pincer complex is an efficient catalyst for concerted removal of H_2 from HBNNT at ambient conditions,[34] in general, non-noble metal containing systems are neither cost-effective nor environment benign which suggests utilization of main group elements beyond the prevalent stoichiometric transformations.[35] We therefore intended to computationally identify a Brønsted acid catalyst which would be more efficacious than triflic acid and can desorb H_2 at room temperature to realize an optimal hydrogen storage-delivery cycle.

Herein, we therefore explore the reaction mechanism of H_2 release from a 1 nm long HBNNT of (8,0) zigzag chirality, catalyzed by several *in silico* designed Brønsted organic acids: 1,1,1-tricyanomethanesulfonic acid [HOSO$_2$C(CN)$_3$] (**A**), 1,1-dicyano-methanesulfonic acid [HOSO$_2$CH(CN)$_2$] (**B**), 1-monocyanomethanesulphonic acid [HOSO$_2$CH$_2$(CN)] (**C**), 1,1,1-trifluoromethanesulphonic acid [HOSO$_2$CF$_3$] (**D**), methanesulphonic acid [HOSO$_2$CH$_3$] (**E**) and 1,1-dicyano-ethanoic acid [HOOCCH(CN)$_2$] (**F**) (see SI1). To be noted that most of these catalysts or their higher chemical analogues are already synthesized commercially, for e.g. trifluoromethanesulphonic acid, methanesulphonic acid, 1,4-Dicyanobutane-2-sulfonic acid, 2,2-Dicyano-2-(2,3-dihydroxypropoxy)acetic acid etc. Indeed, previous reports have outlined several instances where triflic acid and alkyl sulphonic acids are surface functionalized on silica to act as heterogeneous catalysts.[36,37] *In silico* application of these catalysts to delve into uncharted avenues requires a deep chemical knowledge of the crucial intermediates and transition states on the potential energy surface to underscore the key factors that regulate the rate determining state (RDS). State-of-the-art theoretical techniques like the recently developed domain-based local pair natural orbital coupled-cluster approach with single and double excitations and perturbative triple corrections (DLPNO-CCSD(T)) method has been found to be successful in delivering accurate reaction energetics of both homogeneous catalysis[38,39] and also in hybrid QM/MM studies of model enzymatic reactions.[40] Furthermore, DLPNO approach has been demonstrated to be in excellent agreement with explicitly correlated CCSD(T)-F12 method for radical elimination reactions, without compromising with the accuracy of conventional coupled-cluster technique.[41] Hence in the present work, DLPNO-CCSD(T) has been used to compute energetics of critical points on the PES and predict highly accurate activation barriers. Additionally, we have undertaken energetic span analysis to identify the most efficient catalyst of the flock.[42] Evidently, these insights are pivotal for future design of hydrogenation/dehydrogenation catalysts for a sustainable chemical hydrogen storage strategy.

Methods

Optimizations in gas phase were conducted with the B3LYP functional and Pople basis set (B1 basis combination) as implemented in Gaussian 09 quantum chemical package for the full structures of the models as shown in SI1. B1 basis set combination refers to the employment of 6-31++G(d,p) basis for B, N and H atoms in the four adjacent rings at the vicinity of the reaction

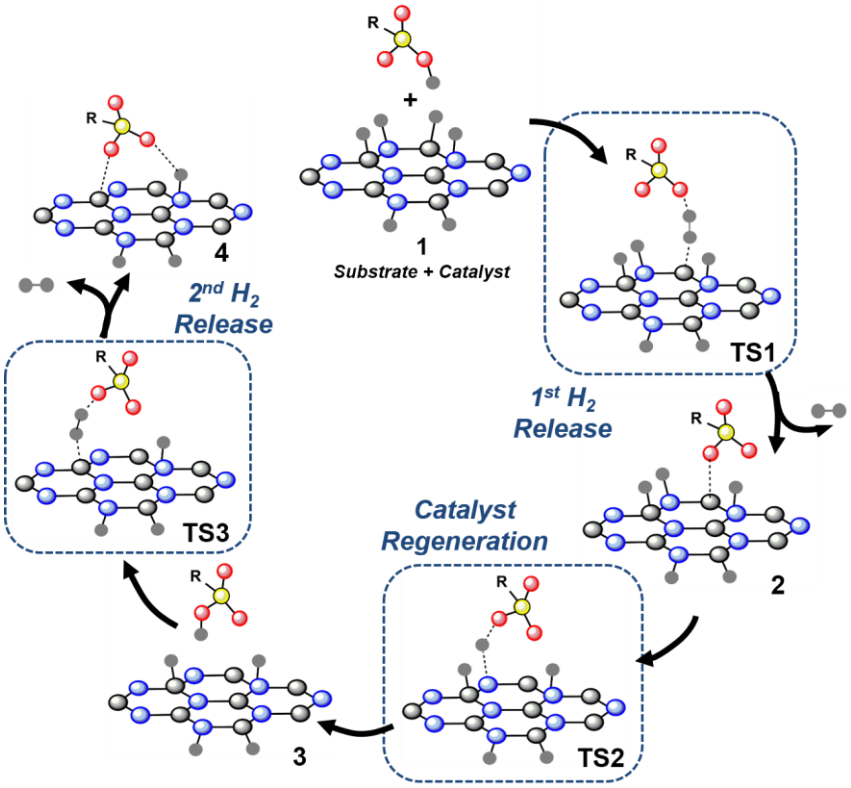

Scheme 1. General catalytic steps proposed for the dehydrogenation of HBNNT by different Brönsted acids. Color code used: N (blue), B (black), H (grey), O (red), S(yellow).

centre on the BNNT surface along with 6-31G(d) for all other atoms. In addition, all the atoms of the Brønsted acid were treated with 6-31++G(d,p) basis set. Harmonic vibrational analyses were conducted at the same level of theory to characterize the structures as minimum (all real frequencies) and transition state (one imaginary mode). Single-point calculations at the DFT optimized geometry was done using DLPNO-CCSD(T) in conjunction with Karslruhe's 2nd generation triple-ζ valence high angular momentum polarization basis set (def2-TZVPP) for more than 3800 basis functions. Interestingly, Neese and co-workers have demonstrated that the relative computational cost for DLPNO-CCSD(T) compared to traditional DFT is only 5 times higher.[38] The TightPNO settings was used all through to achieve a tighter accuracy on the method. The RIJCOSX approximation together with GridX6 was used for the calculation of Coulomb and exchange integrals in the Hartree Fock (HF) reference. The correlation-fitting def2-TZVPP/C auxiliary basis set is used along with the coulomb-fitting def2/J basis set to accelerate the DLPNO-CCSD(T) calculations. For solvent corrections to CC electronic energies, the CPCM model (dielectric constant = 36.6, refractive index = 1.344 for acetonitrile) as implemented in ORCA 4.1 is utilized.[43] Thermal (Temperature = 298.15 K) and non-thermal corrections were obtained from B3LYP frequency calculations. All relative energies and barriers reported in the main text are calculated at DLPNO-CCSD(T)/def2-TZVPP//B3LYP/B1 level of theory. Additional computational details are given in the supporting information.

Results and Discussion

At the onset, we tried to explore the avenue of concerted removal of protons and hydrides to

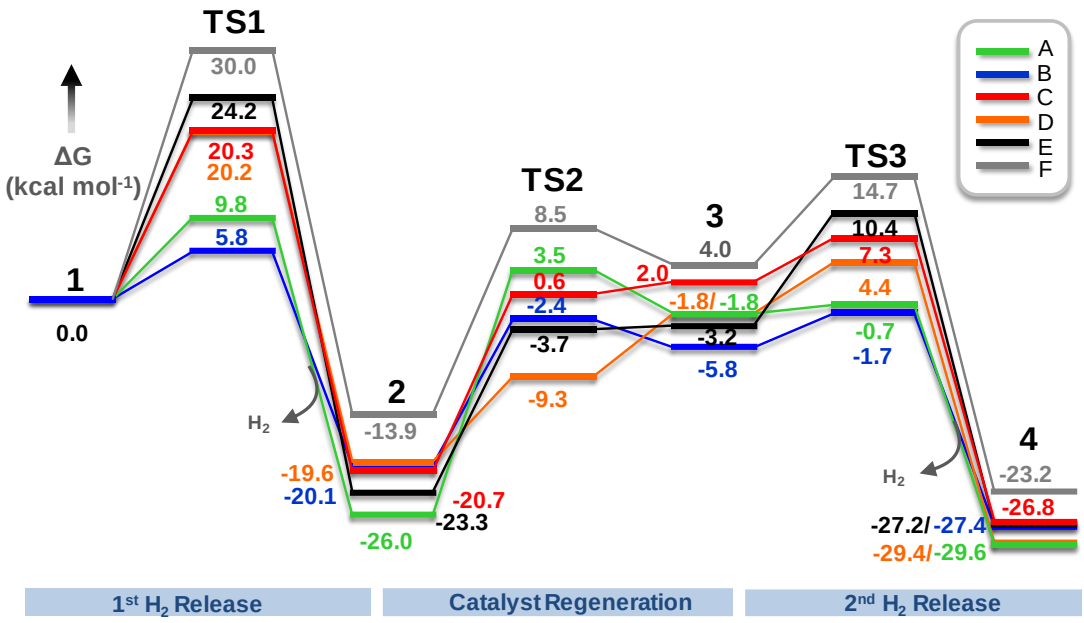

Figure 2. DLPNO-CCSD(T)/def2-TZVPP computed free energy profiles for the key steps of dehydrogenation of HBNNT by different Brønsted acids (**A**-**F**).

release dihydrogen molecule, with application of the acid catalyst, similar to our previous study with Ir-pincer complex.[34] However, the Brønsted acids are not suitable for simultaneous activation of B-H and N-H bonds presumably due to their high acidity which inhibits proton shuttle mechanism.[30] The reaction of all the Brønsted acids considered in this present work follow a common mechanistic paradigm as shown in Scheme 1, previously explored by us for dehydrogenation of HBNNT by catalyst **D**. Following sequences were considered in the present study to ensure sustainability of the process: 1st H_2 release (**1** → **TS1** → **2**), catalyst regeneration (**2** → **TS2** → **3**) and 2nd H_2 release (**3** → **TS3** → **4**) from the substrate, HBNNT. Notably, in previous reports, DLPNO-CCSD(T)/def2-TZVPP calculations has been the chosen method for accurate prediction of barriers consistent with experiments, whereas B3LYP-D3BJ/def2-TZVPP gave erroneous predictions.[39] However, the M06L/def2-TZVPP combination has been found to have similar results as DLPNO-CCSD(T).[39] Hence, in the following sections we discuss the more reliable results with the coupled-cluster theory and summarize the results obtained with DFT in the supporting information (SI2).

The coordination of a catalyst molecule (**A**-**F**) with HBNNT is a free energetically unfavorable process; corresponding reactant complexes with **A** (11.3 kcal mol^{-1}), **B** (9.3 kcal mol^{-1}), **C** (8.7 kcal mol^{-1}), **D** (7.1 kcal mol^{-1}), **E** (8.2 kcal mol^{-1}) and **F** (9.5 kcal mol^{-1}) are significantly endoergic with regard to the separated species and therefore have not been considered in the DLPNO-CCSD(T)/def2-TZVPP free energy profile in Figure 2. Furthermore, formation of acid dimers is also predicted to be free energetically unfavorable (ΔG = 5 – 11 kcal mol^{-1}), (see SI6) suggesting that dimerization would not inhibit reaction of the catalyst with the hydrogenated BN nanotube.[15,25] Additionally, calculations also revealed that for catalyst **F**, dimerization is a thermoneutral process (ΔG = -0.7 kcal mol^{-1}) indicating an equilibrium between acid and its dimer in reaction medium. Hence, it is unlikely

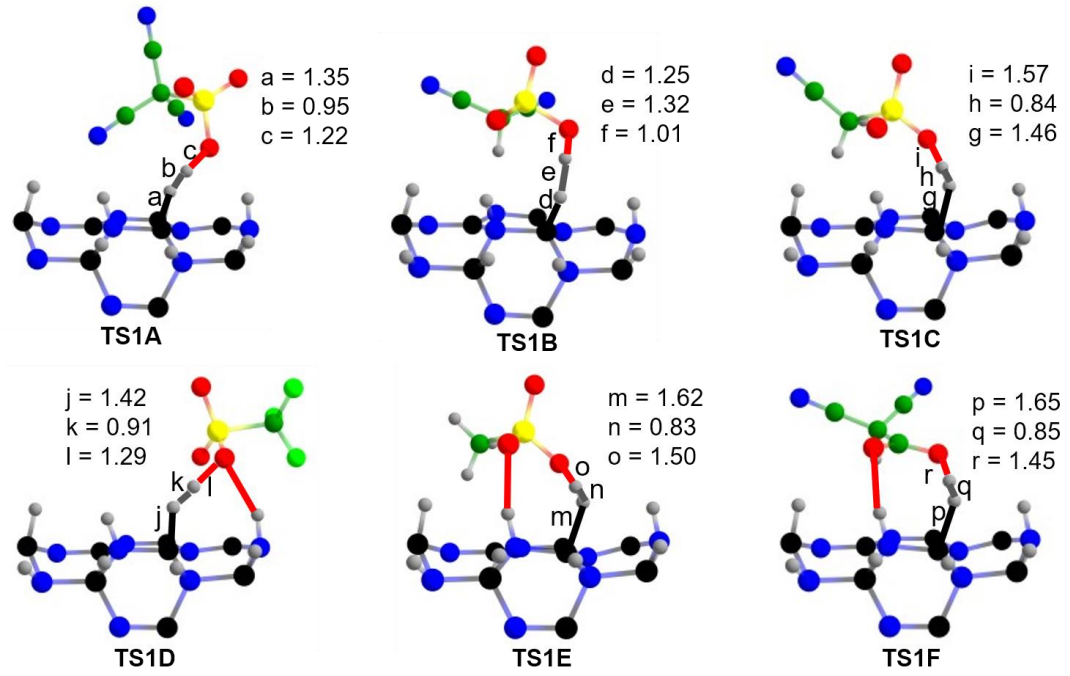

Figure 3. Partial view of the optimized geometry of TS1 with different catalysts (A-F). Color code used: N(blue), B(black), H(grey), O(red), S(yellow), C(deep green), F(light green). Distances reported are in units of Å.

that the Bronsted acids would remain as hydrogen bonded dimers in acetonitrile solvent and were not further considered to react with HBNNT.

The reaction is initiated by protonolysis of a proximal B-H bond by the catalyst to form molecular H_2.[31] The generation and removal of H_2 is a concerted process while a similar reactivity with ammonia borane proceeds through a solvent assisted protonation of the hydride of NH_3BH_3 to form a non-classical boronium cation as predicted earlier with molecular dynamics.[44,45] The release of dihydrogen from $NH_3BH_4^+$ species in the next step results in strong B-O(ether) covalent bond.[44] However, utilization of non-ether solvents like acetonitrile and benzene are expected to minimize such solvent participation and therefore has been introduced in the present study through continuum solvent model. Hereafter we append the name of the catalyst on the intermediate or the transition state to interpret the system under consideration. It is evident from Figure 2 that different degrees of strength of the attached substituents on the acids dramatically alters the barriers. Specifically, introducing higher electron withdrawing -CN groups in **A** and **B** curtails the difficulty in 1st H_2 release by hydride activation through **TS1A** and **TS1B**, with a predicted barrier of 9.8 and 5.8 kcal mol^{-1} respectively as compared to 24.2 kcal mol^{-1} barrier with -CH_3 substituent on the catalyst in **TS1E**. The transition state geometries leading to concomitant B-H activation and dislodge of H_2 are also starkly different with different catalysts.[30,31,44] As observed from Figure 3, the target B-H bond is most elongated in **TS1F** (late transition state) while it is least activated in **TS1B** (early transition state). In fact, the B–H distance in the optimized geometry of the transition state is directly proportional to the predicted barrier; **TS1F**: 1.65 Å; 30.0 kcal mol^{-1}, **TS1E**: 1.62 Å; 24.2

kcal/mol; **TS1C**: 1.57 Å, 20.2 kcal mol^{-1}; **TS1D**: 1.42 Å, 20.2 kcal mol^{-1}; **TS1A**: 1.35 Å; 9.8 kcal mol^{-1}; **TS1B**: 1.25 Å, 5.8 kcal mol^{-1}. This is also in congruence to the global electrophilicity parameter (ω) of the catalyst as shown in Table 1. Interestingly, the electrophilicity marker for catalyst **B** is ~3 times greater than that for catalyst **F**, although they have two -CN groups attached, and therefore catalyst **B** is ~5 times more reactive towards protonation of HBNNT than catalyst **F** (Figure 2 and Table 1). Musgrave *et al.* predicted similar difficulty in B-H activation in an ammonia borane dimer ($\Delta G^{\ddagger}$ = 27.7 kcal mol^{-1}).[46] However, an electrophilic transition metal center like Ru is predicted to carry out B-H activation at a much lower free energetic cost ($\Delta G^{\ddagger}$ = 18.8 kcal mol^{-1}).[47] This observation illustrates that acids with optimum electrophilicity can deliver similar H_2 release reactivity as that of a transition metal center.[17,30,47] Notably, thermal desorption of H_2 from the nanotube surface is predicted at an activation barrier of 42.5 kcal mol^{-1} at DLPNO-CCSD(T)/def2-TZVPP level of theory which further emphasizes on the importance of suitable catalysts or bifunctional reagents to elicit coupling of hydrides and protons on HBNNT.

Table 1. Comparison of H_2 release barrier with global reactivity descriptors at M06L/def2-TZVPP in eV and B-H bond distances in Å.[a]

	B-H bond distance (Å) in **TS1**	global electrophiclitity (*ω*)	H_2 release barrier (kcal mol^{-1})
A	1.35	6.4	9.8
B	1.25	4.6	5.8
C	1.57	3.0	20.0
D	1.42	4.1	17.8
E	1.62	2.2	20.1
F	1.65	1.6	30.0

[a] See SI1 for computational details.

The release of H_2 molecule furnishes a cationic HBBNT and an acid anion. As a result, **1** → **TS1** → **2** transformation is found to follow a huge driving force (-19.0 to -26.0 kcal mol^{-1}) which must originate due to the significant ionic and H-bonding interactions between the two charged fragments (Figure 4a). In a consequent step, the catalyst is regenerated by abstraction of a N-H proton from positively charged HBNNT species by a conjugate base.[30] Proton abstraction by all the Brønsted acid anions are essentially endoergic processes as evident from Figure 2. Hence the overall barrier for acid regeneration by these systems turns out to be 17-29 kcal mol^{-1}. Thus, catalyst regeneration is found to be a crucial step in order to drive the dehydrogenation process forward. Specifically, the decrement of the barrier-height by ~ 12 kcal mol^{-1} on going from **TS2A** to **TS2B** is remarkable and warrants further understanding on the basis of electronic structure theory; hence we conducted local energy decomposition (LED) analysis.[48]

The system under consideration was partitioned as shown in Figure4a into different fragments for the interacting molecules. Decomposition of the total interaction energy (ΔE_{int}) into meaningful contributions like electrostatic (ΔE_{ref}^{elst}), electronic preparation ($\Delta E_{ref}^{el\text{-}prep}$), exchange ($\Delta E_{ref}^{exch}$), dispersion ($\Delta E_{Corr}^{disp}$), non-dispersion ($\Delta E_{corr}^{no\text{-}disp}$) and triples correction ($\Delta E_{Corr}^{C\text{-}(T)}$) was done as shown in Table 2 [49] to provide insight into the electronic factors that contribute to the destabilization of the transition states (TSs) as compared to their respective reactant complexes (RCs) (see SI1 for details).[50] ΔE_{ref}^{elst} furnishes the degree of changes in Coulombic interactions between the electronic clouds of the interacting fragments in the RCs as compared to that in the distorted electronic clouds of the TSs, taking into consideration both permanent and induced electrostatic energy. On the other hand, $\Delta E_{ref}^{el\text{-}prep}$ is the difference in the energy required to bring the electrons of the two fragments into an optimal structure in the RC compared to that in the TS. ΔE_{ref}^{exch} is the relative stabilizing intermolecular exchange component. $\Delta E_{corr}^{no\text{-}disp}$ delivers the correction to the permanent and induced electrostatics due to the correlation contributions arising from instantaneous

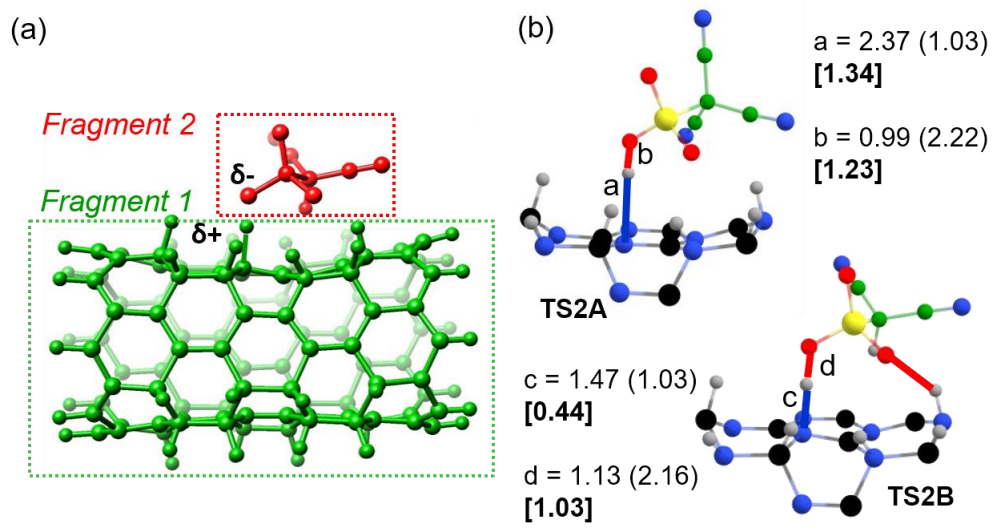

Figure 4. (a) Fragmentation of the system under consideration for LED investigation. (b) Partial view of the optimized geometry of TS2A and TS2B. Distances reported are in units of Å. Corresponding distances in the respective RCs are given in parenthesis while Δ value in third-bracket. Color code used: N(blue), B(black), H(grey), O(red), S(yellow), C(deep green).

cationic-anionic pair. The weak dispersive correlation energy of distant electronic pairs is given by ΔE_{Corr}^{disp} while $\Delta E_{Corr}^{C-(T)}$ is the contribution of the triples correction to the correlation energy. From Table 2 it is evident that ΔE_{ref}^{elst} and $\Delta E_{ref}^{el-prep}$ are the major contributors to the total interaction energy difference. In both the cases, the electrostatic interaction energy difference is >100 kcal mol^{-1} suggesting that there is a huge drop in the attractive Coulombic interactions on going from the RC to the TS. This is because in the RC, the two fragments are oppositely charged; as they approach each other closer and reach the TS, they are transformed into two neutral species. ΔE_{ref}^{elst} of 164 kcal mol^{-1} for **2B/TS2B** pair as compared to much diminished 100 kcal/mol for **2A/TS2A** pair further indicates that the sum of electrostatics in **2B** is significantly greater than that in **2A**. However, this is compensated to a great extent by the stability gained in electronic arrangement ($\Delta E_{ref}^{el-prep}$) in the TS as compared to the RC. Particularly, this stability gain is more for **2B/TS2B** pair (-140 kcal mol^{-1}) than **2A/TS2A** pair (-46.4 kcal mol^{-1}). Indeed, a comparison of the important bond lengths in both these pairs (Figure 4b) also indicate a greater extent of geometric reorganization in **TS2A**, referenced to

Table 2. Local energy decomposition of DLPNO-CCSD(T)/def2-TZVPP energies in kcal mol^{-1} for catalyst regeneration step (**TS2**) for catalyst type **A** and **B**.

Species	ΔE_{int}	ΔE_{ref}^{elst}	$\Delta E_{ref}^{el-prep}$	ΔE_{ref}^{exch}	ΔE_{Corr}^{disp}	$\Delta E_{corr}^{no-disp}$	$\Delta E_{corr}^{no-disp}$	$\Delta E_{Corr}^{C-(T)}$
A	34.5	100.9	-46.4	0.6	-3.8	-13.6	-13.6	-3.1
B	23.5	164.4	-140.5	8.1	1.1	-8.1	-8.1	-1.5

2A, than in the other analogue. The non-dispersive correlation correction to the attractive electrostatics to some extent tackle down the adverse effect of Hartree-Fock reference in **2A/TS2A**.[48,49] However, contributions from other inter-fragment interactions are paltry as shown in Table 2. Taken together, the interaction energy between the two fragments in both the pairs is repulsive all along the path: **2 → TS2**.[50] However, all these intermolecular interactions are more balanced for **2B/TS2B** which results in the significant decrease in the overall barrier height, thus emphasizing on the optimum acidity of the molecule to account for a feasible regeneration.

Table 3. Energetic span analysis

Catalyst	TDI	TDTS	δE (kcal mol^{-1})	TOF(s^{-1})
A	2A	TS2A	29.5	1.4 x 10^{-11}
B	2B	TS2B	17.7	2.8 x 10^{-2}
C	2C	TS3C	28.0	2.2 x 10^{-9}
D	2	TS3D	24.0	3.5 x 10^{-6}
E	3	TS3E	33.7	6.0 x 10^{-14}
F	1	TS1F	30.0	5.4 x 10^{-12}

The revival of the catalyst indicates the possibility of removal of another H_2 to ensure sustainability of the dehydrogenation process. The lowest energy pathway for 2nd H_2 release is observed in the case of catalyst **B**, with the intermediacy of **TS3B** ($\Delta G^{\ddagger}$ = 18.4 kcal mol^{-1}), where reformation of the catalyst instigates protonation of a neighboring B-H bond. Conversely, for all the other species, the 2nd H_2 release barrier is raised by ~ 6-15 kcal mol^{-1} which highlights that it is rather difficult to design a viable dehydrogenation process with the alternatives. Indeed, an in-depth analysis of the three reaction steps shown in Scheme 1 and Figure 2 has been done with the popular energetic span model (ESM) (see SI1).[42] This approach characterizes the rate-determining intermediates and transition states to analyze the efficiency of a catalytic process and figure out the most favorable pathway.[51] As found from the free energy profiles in Figure 2 and Table 3, the proton abstraction by acid anion for catalyst regeneration is the turn-over determining transition state (TDTS) and turn-over determining intermediate (TDI) for catalyst type **A** and **B,** viz. **TS2A** and **TS2B**. For catalysts **C-E**, the 2nd H_2 release step is the TDTS. The energetic span (δE) for the latter processes are predicted to be 24.0 – 33.7 kcal mol^{-1} with TOF in the range of 10^{-9} to 10^{-14} s^{-1}. For only catalyst **F**, **TS1F** is the TDTS with δE = 30.0 kcal mol^{-1}. From Table 3 it is evident that catalyst **B** shows the highest efficiency for the three consecutive reaction steps, overcoming the reactivity of our earlier studied model catalyst, triflic acid (**D**), by almost 10^4 times. Furthermore, a plot of the logarithm of the TOF for the TDTS illustrated in Figure 5 shows the following trend for catalytic efficiency: **B** > **D** > **C** > **A** > **F** > **E**. These observations provide a proof of principle how the catalytic efficiency for dehydrogenation of HBNNT could be significantly improved by modifying the electrophilic nature of the acid. It further portrays how computational explorations could lead to better ideas for designing dehydrogenation catalysts.[52]

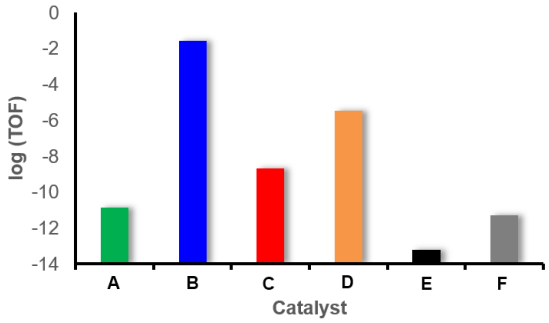

Figure 5. Plot of the logarithm of the TOF for the TDTS with different catalysts.

One may fathom that with decrease in the chemisorbed hydrogen content, the possibility of dehydrogenation would be curtailed. Hence, to ensure continuous removal of H_2 molecules from HBNNT we have studied dehydrogenation from low hydrogen weight containing BN nanotube surface with the most

effective catalyst, B. We selected a single hydrogenated hexagonal BN unit at the middle of HBNNT and found that removal of H_2 molecule with **B** is a feasible process at $\Delta G^{\ddagger}$ = 16.8 kcal mol^{-1} via $\mathbf{TS1_L}$ (SI3). This result surely indicates the possibility of removal of all the hydrogen from HBNNT at room temperature, with application of the acid catalyst, **B**. These promising developments encouraged us to test the viability of the proposed dehydrogenation process with different BN nanostructures and therefore we chose an armchair (3,3) BN cluster with hydrogenated terminals (h-BN). The initial proton-hydride coupling on h-BN to release H_2 in presence of the Brønsted acid, B, with $\Delta G^{\ddagger}$ = 12.8 kcal mol^{-1} is certainly comparable to **TS1B**. Furthermore, acid regeneration in h-BN ($\Delta G^{\ddagger}$ = 14.0 kcal mol^{-1}) also follows a similar trend as **TS2B**. Hence we predict that removal of hydrogen from both HBNNT and h-BN would be possible at room temperature, if we employ appropriate catalytic agents like **B**, while thermal desorption of H_2 takes place at > 300 °C. Our findings surely indicate the possibility of development of viable dehydrogenation technology[27] from chemical hydrogen storage media with application of acid initiators.

Conclusions

In conclusion, we outline a strategy to design effective metal free Brønsted acid as catalysts for dehydrogenation of hydrogen storage materials like BN nanotube. The transition state barriers with highly accurate DLPNO-CCSD(T)/def2-TZVPP level of theory with different Brønsted acids certainly sugests that proper screening of catalysts can initialize H2 removal and ensure chain reactions at room temperature, overcoming the kinetic trap associated with thermal release of dihydrogen from BN nanotubes. Our calculations reveal that 1,1-dicyano-methanesulfonic acid [$HOSO_2CH(CN)_2$] is a potential catalyst suitable for application under ambient conditions. It is found to conform to a balance between dehydrogenation and catalyst regeneration reactions due to its inherent electronic properties. The low barrier pathway ($\Delta G^{\ddagger}$= 17 kcal mol^{-1}) found with removal of chemisorbed hydrogen atoms from BN nanotube by this acid raise hope for a sustainable hydrogenation/dehydrogenation process at room temperature. Additionally, the current work represents how a computational approach can be utilized to screen plausible catalysts and consort to the most efficient candidate for further experimental investigations.

Funding Information

Department of Science and Technology, India (DST/INSPIRE/04/2017/000446) and start-up research grant, Institute of Chemical Technology Mumbai – IOC Odisha Campus Bhubaneswar.

Keywords: dehydrogenation • nanotubes • main group elements • ab initio calculations • catalysis

Additional Supporting Information may be found in the online version of this article.

References and Notes

1. C. L. Aardahl, S. D. Rassat, *Int. J. Hydrogen Energy* **2009**, *34*, 6676−6683.
2. C. A. Dillon; K. M. Jones, T. A. Bekkedahl, C. H. Kiang, D. S. Bethune, M. J. Heben, *Nature*, **1997**, *386*, 377 – 379.
3. H. Lee, J.–w. Lee, D. Y. Kim, J. Park, Y.-T. Seo, H. Zeng, I. L. Moudrakovski, C. I. Ratcliffe, J. A. Ripmeester, *Nature* **2005**, *434*, 743 – 746.
4. Z. Xiong, C. K. Yong, G. Wu, P. Chen, W. Shaw, A. Karkamkar, T. Autrey, M. O. Jones, S. R. Johnson, P. P. Edwards, W. I. F. David, *Nat. Mater.* **2008**, 7, 138-141.

5. Y. Zhao, Y.-H. Kim, A. C. Dillon, M. J. Heben, S. B. Zhang, *Phys. Rev. Lett.* **2005**, *94*, 155504.
6. N. L. Rosi, J. Eckert, M. Eddaoudi, D. T. Vodak, J. Kim, M. O'Keeffe, O. M. Yaghi, *Science* **2003**, *300*, 1127-1129.
7. X. Liang, S.-P. Ng, N. Ding, C.-M. L. Wu, *Appl. Surf. Sci.* **2019**, *473*, 174-181.
8. E. Tsivion, J. R. Long, M. Head-Gordon, *J. Am. Chem. Soc.* **2014**, *136*, 17827−17835.
9. V. Tozzini, V. Pellegrini, *Phys. Chem. Chem. Phys.* **2013**, *15*, 80-89.
10. S. Orimo, Y. Nakamori, J. R. Eliseo, A. Züttel, C. M. Jensen, *Chem. Rev.* **2007**, *107*, 4111 – 4132.
11. C. W. Hamilton, R. T. Baker, A. Staubitz, I. Manners, *Chem. Soc. Rev.* **2009**, *38*, 279−293.
12. R. J. Keaton, J. M. Blacquiere, R. T. Baker, *J. Am. Chem. Soc.* **2007**, *129*, 1844−1845.
13. A. Paul, C. B. Musgrave, *Angew. Chem., Int. Ed.* **2007**, *46*, 8153 – 8156.
14. G. Menard, D. W. Stephan, *J. Am. Chem. Soc.* **2010**, *132*, 1796−1797.
15. L. Roy, P. M. Zimmerman, A. Paul, *Chem. - Eur. J.* **2011**, *17*, 435−439.
16. K. Mori, K. Miyawaki, H. Yamashita, *ACS Catal.* **2016**, *6*, 3128 – 3135.
17. L. Roy, B. Ghosh, A. Paul, *J. Phys. Chem. A* **2017**, *121*, 5204−5216.
18. M. C. Denney, V. Pons, T. J. Hebden, D. M. Heinekey, K. I. Goldberg, *J. Am. Chem. Soc.* **2006**, *128*, 12048 – 12049.
19. A. D. Sutton, A. K. Burrel, D. A. Dixon, E. B. Garner III, J. C. Gordon, T. Nakagawa, K. C. Ott, J. P. Robinson, M. Vasilliu, *Science* **2011**, *331*, 1426−1429.
20. R. Ma, Y. Bando, H. Zhu, T. Sato, C. Xu, D. Wu, *J. Am. Chem. Soc.* **2002**, *124*, 7672−7673.
21. C. Tang, Y. Bando, X. Ding, S. Qi, D. Golberg, *J. Am. Chem. Soc.* **2002**, *124*, 14550 – 14551.
22. D. Golberg, Y. Bando, Y. Huang, T. Terao, M. Mitome, C. Tang, C. Zhi, *ACS Nano* **2010**, *4*, 2979 – 2993.
23. D. Golberg, Y. Bando, C. Tang, C. Zhi, *Adv. Mater.* **2007**, *19*, 2413 – 2432.
24. E. M. Kumar, S. Sinthika, R. Thapa, *J. Mater. Chem. A* **2015**, *3*, 304 – 313.
25. S.-H. Wen, W.-Q. Deng, K. L. Han, *J. Phys. Chem. C* **2008**, *112*, 12195 – 12200.
26. J. Li, J. Lin, X. Xu, X. Zhang, Y. Xue, J. Mi, Z. Mo, Y. Fan, L. Hu, X. Yang, J. Zhang, F. Meng, S. Yuan, C. Tang, *Nanotechnology*, **2013**, *24*, 155603.
27. A. Lale, S. Bernard, U. B. Demirci, *ChemPlusChem* **2018**, *83*, 893 – 903.
28. W. Lubitz, E. Reijerse, M. van Gastel, *Chem. Rev.* **2007**, *107*, 4331 – 4365.
29. L. Roy, S. Mittal, A. Paul, *Angew. Chem. Int. Ed.* **2012**, *51*, 4152 – 4156.
30. L. Roy, S. Bhunya, A. Paul, *Angew. Chem. Int. Ed.* **2014**, *53*, 12430 – 12435.
31. F. H. Stephens, R. T. Baker, M. H. Matus, D. J. Grant, D. A. Dixon, *Angew. Chem. Int. Ed.* **2007**, *46*, 746 – 749.
32. P. Bhattacharya, J. A. Krause, H. Guan, *J. Am. Chem. Soc.* **2014**, *136*, 11153 – 11161.
33. B. L. Conley, D. Guess, T. J. Williams, *J. Am. Chem. Soc.* **2011**, *133*, 14212 – 14215.
34. L. Roy, A. Paul, *Chem. Commun.*, **2015**, *51*, 10532 – 10535.
35. N. A. Sitte, M. Bursch, S. Grimme, J. Paradies, *J. Am. Chem. Soc.* **2019**, *141*, 159−162.
36. D. C. Rosenfeld, S. Shekhar, A. Takemiya, M. Utsunomiya, J. F. Hartwig, *Org. Lett.* **2006**, *8*, 4179 – 4182.
37. Z. Li, J. Zhang, C. Brouwer, C.-G. Yang, N. W. Reich, C. He, *Org. Lett.* **2006**, *8*, 4175 – 4178.
38. B. Mondal, F. Neese, S. Ye, *Inorg. Chem.* **2015**, *54*, 7192−7198.
39. L. Roy, M. H. Al-Afyouni, D. E. DeRosha, B. Mondal, I. M. DiMucci, K. M. Lancaster, J. Shearer, E. Bill, W. W. Brennessel, F. Neese, S. Ye, P. L. Holland, *Chem. Sci.* **2019**, *10*, 918–929.
40. G. Bistoni, I. Polyak, M. Sparta, W. Thiel, F. Neese, *J. Chem. Theory Comput.* **2018**, *14*, 3524−3531.

41. V. G. Kiselev, F. C. Goldsmith, *J. Phys. Chem. A* **2019**, *123*, 4883−4890.
42. S. Kozuch, S. Shaik, *Acc. Chem. Res.* **2011**, *44*, 101−110.
43. F. Neese, *WIREs Comput. Mol. Sci.* **2018**, *8*, e1327.
44. S. Bhunya, A. Banerjee, R. Tripathi, N. N. Nair, A. Paul, *Chem. Eur. J.* **2013**, *19*, 17673 – 17678.
45. D. H. A. Boom, A. R. Jupp, J. C. Slootweg, *Chem. Eur. J.* **2019**, *25*, 9133 – 9152.
46. P. M. Zimmerman, Z. Zhang, C. B. Musgrave, *J. Phys. Chem. Lett.* **2011**, *2*, 276 – 281.
47. S. Bhunya, L. Roy, A. Paul, *ACS Catal.* **2016**, *6*, 4068−4080.
48. W. B. Schneider, G. Bistoni, M. Sparta, M. Saitow, C. Riplinger, A. A. Auer, F. Neese, *J. Chem. Theory Comput.* **2016**, *12*, 4778−4792.
49. A. Altun, M. Saitow, F. Neese, G. Bistoni, *J. Chem. Theory Comput.* **2019**, *15*, 1616 – 1632.
50. Y. Cornaton, J.-P. Djukic, *Phys. Chem. Chem. Phys.* **2019**, *21*, 20486-20498.
51. L. Roy, *ChemCatChem* **2018**, *10*, 3683 – 3688.
52. L. Roy, *ChemPlusChem* **2019**, *84*, 893 – 906.